BEAM ECHO EFFECT FOR GENERATION OF SHORT-WAVELENGTH RADIATION*

G. Stupakov, SLAC National Accelerator Laboratory, Menlo Park, CA, USA

Abstract

The Echo-Enabled Harmonic Generation (EEHG) FEL uses two modulators in combination with two dispersion sections to generate a high-harmonic density modulation starting with a relatively small initial energy modulation of the beam. After presenting the concept of the EEHG, we address several practically important issues, such as the effect of coherent and incoherent synchrotron radiation in the dispersion sections. Using a representative realistic set of beam parameters, we show how the EEHG scheme enhances the FEL performance and allows one to generate a fully (both longitudinally and transversely) coherent radiation. We then discuss application of the echo modulation for generation of attosecond pulses of radiation, and also using echo for generation of terahertz radiation. We present main parameters of a proof-of-principle experiment currently being planned at SLAC for demonstration of the echo modulation mechanism.

INTRODUCTION

There has been continually growing interests in generating coherent and powerful short wavelength radiation using the free electron laser (FEL) scheme, as reflected by the many proposals and funded projects worldwide [1]. In the nanometer and sub-nanometer wavelengths, the two leading candidates are self-amplified spontaneous emission (SASE) configuration [2, 3] and the high gain harmonic generation (HGHG) scheme [4, 5]. Since the SASE FEL starts from electron beam shot noise, its output typically has limited temporal coherence and relatively large shot-to-shot fluctuations in both the power and the spectrum. An alternative to SASE configuration is the HGHG scheme that allows generation of temporally coherent radiation by using up-frequency conversion of a high-power seeding signal.

In the classic HGHG scheme [5], the electron beam is first energy modulated with a seed laser in the undulator (modulator) and then sent through a dispersion region which converts the energy modulation into a density modulation. The density modulated beam is then sent through the second undulator (radiator) tuned at some harmonic of the seed laser. The up-frequency conversion efficiency for this classic HGHG scheme is relatively low: generation of nth harmonic of the seed laser requires the energy modulation amplitude approximately equal to n times the slice energy spread of the beam. Because a considerable increase of the slice energy spread would significantly degrade the lasing process in the radiator, the harmonic numbers n used in the classic HGHG scheme are typically no larger than 6. In order to generate coherent soft x-rays with a wavelength in the range of few nanometers using an ultra-violet (UV) seeding laser with the wavelength ~ 200 nm, multiple stages of the classic HGHG FEL are to be used [6].

In order to get higher harmonics while keeping the energy spread growth within acceptable level, a double-undulator HGHG scheme was recently suggested [7] where the modulator is subdivided into two pieces with a π phase shifter between them. This allows for generation of substantial bunching at higher harmonics while simultaneously limiting the growth of the energy spread. However, the double-undulator HGHG scheme still requires a high laser power and small beam slice energy spread, which may limit its practical applications.

Recently a new method for generation of high harmonics using the beam echo effect was proposed [8]. The echo scheme has a remarkable up-frequency conversion efficiency and allows for generation of high harmonics with a relatively small energy modulation. The echo scheme uses two modulators and two dispersion sections. In general, the frequencies of the first, ω_1, and the second, ω_2, modulators can be different. The beam modulation is observed at the wavelength $2\pi/k_{\rm echo}$, where $ck_{\rm echo} = n\omega_1 + m\omega_2$, with n and m integer numbers. The first dispersion section is chosen to be strong enough, so that the energy and the density modulations induced in the first modulator are macroscopically smeared due to the slippage effect. At the same time, this smearing introduces a complicated fine structure into the phase space of the beam. The echo then occurs as a recoherence effect caused by the mixing of the correlations between the modulation in the second modulator and the structures imprinted onto the phase space by the combined effect of the first modulator and the first dispersion section. The key advantage of the echo scheme is that the amplitude of high harmonics of the echo is a slow decaying function of the harmonic number.

HARMONIC GENERATION IN HGHG

In traditional approach to harmonic generation [4, 5], the beam passes through an undulator-modulator and a dispersive element (chicane). A laser pulse in tune with the frequency of the beam radiation in the undulator and synchronized with the beam, modulates the beam energy with the amplitude ΔE and the laser wavelength λ_L. After passage through the chicane with dispersive strength R_{56}, the beam

* Work supported by the U.S. Department of Energy under contract DE-AC02-76SF00515.

gets modulated in density with period λ_L. This modulation carries various harmonics with the wavelength λ_L/k, where k is an integer number. The modulation strength at harmonic k is characterized by the bunching factor b_k defined so that the modulated current $I(z)$ is

$$I(z)/I_0 = 1 + \sum_{k=1}^{\infty} 2b_k \cos(2\pi k z/\lambda_L)\,, \qquad (1)$$

where I_0 is the uniform initial beam current, and z is the longitudinal coordinate in the beam. Assuming a Gaussian energy distribution of the beam with the rms spread σ_E, a simple expression can be obtained for b_k [5]. It follows from that expression that the optimal value of the dispersion approximately satisfies $R_{56}\Delta E/E_0 \approx \lambda_L/4$ (assuming $\Delta E \gg \sigma_E$), where E_0 is the beam energy. With this optimized dispersion strength, in the limit of large k, the absolute value of the bunching factor is

$$|b_k| \approx \frac{0.68}{k^{1/3}} e^{-\frac{k^2}{2A^2}}\,, \qquad (2)$$

where $A = \Delta E/\sigma_E$.

It follows from this formula that if $A \lesssim 1$, then b_k decays exponentially when k increases. To achieve large values of k, it is required that $A \gtrsim k$. However, very large values of A would increase the slice energy spread in the beam and result in the degradation of the lasing process in the radiator.

PRINCIPLES OF EEHG FEL

The schematic of the EEHG is shown in Fig. 1. The EEHG consists of two modulators and two dispersion sections. The system is followed by a radiator undulator (not shown in Fig. 1). Similar to the classic HGHG scheme, a laser pulse is used to modulate the beam energy in the first undulator, and then the beam passes through the first chicane. After that a second laser pulse modulates the beam energy in the second undulator and the beam passes through the second chicane. The laser frequencies for the first and the second modulators, ω_1 and ω_2, in general case are different, but they can also be equal.

Calculations show [8] that at the exit from the second chicane the beam is modulated in the longitudinal direction with the combination of frequencies ω_1 and ω_2. More precisely, the modulations have wavenumbers $k_{n,m}$,

$$ck_{n,m} = n\omega_1 + m\omega_2\,, \qquad (3)$$

where n and m are integer numbers. Note that n and m can be either positive or negative, with a negative $k_{n,m}$ meaning a modulation with wavelength $2\pi/|k_{n,m}|$. Using the notation $b_{n,m}$ for the corresponding bunching factor, one finds [9]

$$b_{n,m} = \Big| e^{-\frac{1}{2}(nB_1+(Km+n)B_2)^2} J_m\left(-(Km+n)A_2B_2\right) J_n\left(-A_1\left(nB_1+(Km+n)B_2\right)\right)\Big|\,, \qquad (4)$$

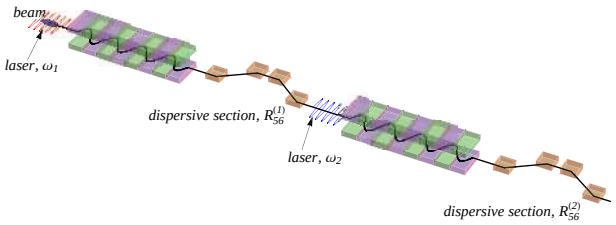

Figure 1: Schematic of the EEHG. The beam energy is modulated in the first undulator (modulator 1) tuned at frequency ω_1 due to the interaction with the first laser beam. After passing through the first dispersion section with $R_{56}^{(1)}$, the beam energy is then modulated in the second undulator (modulator 2) tuned at frequency ω_2 due to the interaction with the second laser beam. The beam then passes through the second dispersion section $R_{56}^{(2)}$.

where $A_1 = \Delta E_1/\sigma_E$, $B_1 = R_{56}^{(1)}k_1\sigma_E/E_0$, $A_2 = \Delta E_2/\sigma_E$, $B_2 = R_{56}^{(2)}k_1\sigma_E/E_0$, ΔE_1 and ΔE_2 are the amplitudes of the energy modulation in the first and second modulators, respectively, $R_{56}^{(1)}$ and $R_{56}^{(2)}$ are the R_{56} parameters for the first and second chicanes, $k_1 = \omega_1/c$, $K = \omega_2/\omega_1$, and J_n is the Bessel function of order n.

Having four dimensionless parameters A_1, A_2, B_1, and B_2 in the problem allows a much better optimization of the absolute value of the bunching factor $b_{n,m}$ for given n, m, and the ratio K of the frequencies. Analysis shows that the bunching factor attains its maximum when $n = \pm 1$ and decreases as the absolute value of n increases. In order for B_1 and B_2 to have the same sign, (which means that one can use either two chicanes or two doglegs as dispersion elements), n and m need to have opposite signs. Limiting our consideration by the case $n = -1$ and $m > 0$ only, we find

$$b_{-1,m} = \big|J_m\left((Km-1)A_2B_2\right) J_1\left(A_1\left(B_1-(Km-1)B_2\right)\right) e^{-\frac{1}{2}(B_1-(Km-1)B_2)^2}\big|\,. \qquad (5)$$

For a given amplitudes A_1 and A_2 and the number m one can try to choose the dispersion strengths B_1 and B_2 in such a way that they maximize the value of $b_{-1,m}$. Such maximization was carried out in Ref. [9]. For $m > 4$, the optimal value of B_2 is given by

$$B_2 = \frac{m + 0.81m^{1/3}}{(Km-1)A_2}\,. \qquad (6)$$

After B_2 is found, the optimal value of B_1 is computed from

$$B_1 = (Km-1)B_2 + \xi(A_1)\,, \qquad (7)$$

where the function $\xi(A_1)$ should be determined from the equation $A_1\left[J_0(A_1\xi) - J_2(A_1\xi)\right] = 2\xi J_1(A_1\xi)$. When

both conditions (6) and (7) are satisfied, it turns out that the bunching factor does not depend on A_2 and depends only on A_1. This dependence is given by the following equation

$$b_{-1,m} \approx \frac{F(A_1)}{m^{1/3}}\,, \tag{8}$$

where the function $F(A_1)$ is shown in Fig. 2. From Fig. 2

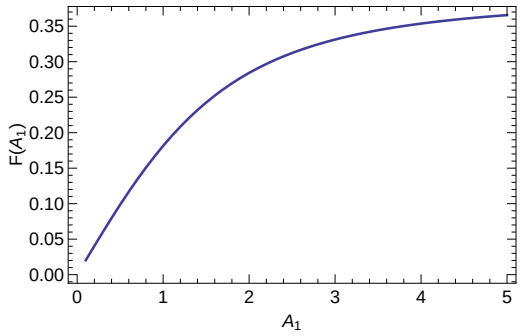

Figure 2: The dependence F from Eq. (8) versus A_1.

one sees that the maximal value of this function increases linearly with A_1 when A_1 is smaller than 2. When A_1 becomes larger than 3, the growth of F slows down, and when A_1 tends to infinity, F approaches 0.39. In this limit the maximal bunching factor becomes (assuming $m > 4$)

$$b_{-1,m} \approx \frac{0.39}{m^{1/3}}\,. \tag{9}$$

Comparing (9) with (2) we see the main advantage of the echo scheme: it allows one to achieve a high modulation at a large harmonic without excessive increase of the modulation amplitude A_1.

Note that if ω_1 and ω_2 are commensurate (and in particular case are equal), not all values $k_{n,m}$ given by (3) are different. For example, if $\omega_1 = \omega_2$, all the values of n and m such that $n + m = \text{const}$ give the same wave number $k_{n,m}$. In this case, the expression (4) should be replaced by the sum of the terms that have the same $k_{n,m}$. In the optimized condition, however, it turns out that typically only one term in this sum dominates, and the analysis presented above remains valid.

ECHO PHASE SPACE

As follows from Eqs. (6) and (7), in the limit of large values of m, and assuming $A_1, A_2 \sim 1$,

$$B_2 \approx \frac{1}{KA_2}\,, \qquad B_1 \approx \frac{m}{A_2}\,, \tag{10}$$

which means that the strength of the first chicane becomes large (note that for the harmonic generation in HGHG discussed above, the optimal value of R_{56} in our units is given by $B \approx \pi/2A$). The large value of $R_{56}^{(1)}$ results in dramatic changes of the longitudinal phase space of the beam. The phase space and the energy distribution function after the first chicane for $B_1 = 12.1$ and $A_1 = 1$ are shown in Fig. 3. The complicated structure of the phase space results from

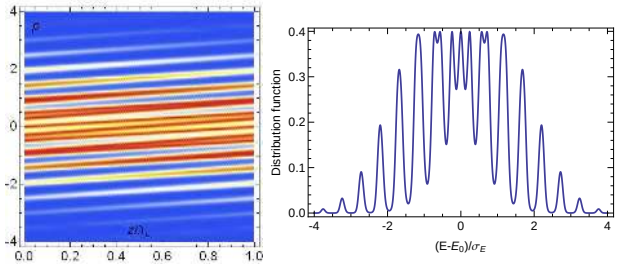

Figure 3: Longitudinal phase space of the beam after passage through the first chicane (left panel) and the corresponding energy distribution of the beam (right panel). The vertical axis on the left panel shows the dimensionless deviation of the energy $p = (E - E_0)/E_0$, and the horizontal axis is the longitudinal coordinate z normalized by the laser wavelength λ_L. The energy distribution is calculated for position $z/\lambda_L = 0.5$.

the fact that due to large slippage of particles with different energies, they end up at the same position z starting many wavelengths away from that position. Correspondingly, the energy distribution function becomes highly modulated in energy, as is shown in Fig. 3. Note also that, if projected onto the z axis, the distribution function in Fig. 3 does not show any density of current modulation.

A subsequent modulation of the beam energy in the second undulator and the passage through the second chicane result in the phase space shown in Fig. 4, for $A_2 = 1$ and $B_2 = 1.3$. The stripes in the phase space of Fig. 3 are

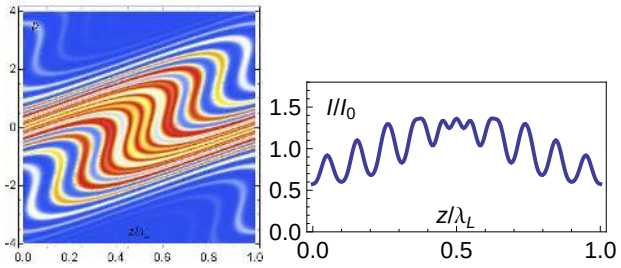

Figure 4: Longitudinal phase space of the beam after passing through the second chicane (left panel) and the corresponding current distribution of the beam (right panel). The current distribution is shown for one period of modulation λ_L.

now stretched and rotated by ninety degrees in their middle parts in such a way that their projections onto the z axis generate modulation of the beam density and current. The corresponding current modulation is shown in the right panel of Fig. 4: the maximal harmonic bunching factor in this modulation corresponds to the harmonic $k = 10$ with

the bunching factor $b_{10} \approx 0.08$.

PRACTICAL PARAMETERS

To illustrate a possible application of the EEHG in a system with realistic parameters, we take the nominal parameters of the Fermi@Elettra FEL project [10] and show below how the 24th harmonic of the seed laser can be generated with a relatively small energy modulation using the EEHG scheme. The electron beam energy of the Fermi@Elettra FEL is 1.2 GeV and the slice energy spread is 150 keV. We assume the wavelength of the seed laser 240 nm with the frequency of the first and the second modulators equal, $\omega_1 = \omega_2$. The energy modulation amplitudes in modulator 1 and modulator 2 are chosen to be $A_1 = 3$ and $A_2 = 1$, respectively. Note that the energy modulation amplitude in our example is much smaller than the nominal value of the modulation amplitude in the Fermi@Elettra project. The optimized dispersion strengths obtained from Eqs. (6) and (7) that maximize the bunching factor for the 24th harmonic are found to be $B_1 = 26.83$ and $B_2 = 1.14$, corresponding to $R_{56}^{(1)} = 8.20$ mm and $R_{56}^{(2)} = 0.35$ mm, respectively. The maximal displacement of the electrons in the longitudinal direction after passing through the first dispersion section is about $A_1 B_1 / k \approx 13\lambda_L$ that is small compared to the overall bunch length.

In Table 1, in addition to the example presented above, we show two more sets of parameter, which can be used for beam modulation at 24th as well as 48th harmonics of the laser. Note that increasing A_2 from 1 to 3 in case $\lambda_r = 10$ nm makes the strength of the first chicane 3 times smaller (the second line in the table). Also note that with $A_2 = 2$, the parameters of the first chicane for generation of the 48th harmonic is close to that for the 24th harmonic (and the second chicane is actually weaker for the shorter wavelength).

k	b_k	λ_r	A_1	A_2	$R_{56}^{(1)}$	$R_{56}^{(2)}$
24	0.11	10	3	1	8.2	0.35
24	0.11	10	3	3	2.5	0.12
48	0.09	5	3	2	8.1	0.16

Table 1: Possible EEHG parameters for the Fermi@Elettra FEL parameters: k is the harmonic number, b_k is the bunching factor, λ_r is the wavelength of the microbunching in nanometers, $R_{56}^{(1)}$ and $R_{56}^{(2)}$ are the chicane strengths in millimeters.

ISSUES AFFECTING EEHG

There are many practical considerations that were neglected in the simple one-dimensional model of EEHG developed in the previous sections. Among the most important of them are the incoherent synchrotron radiation (ISR) and the coherent synchrotron radiation (CSR) of the beam in dipole magnets of the dispersive elements of the system.

Due to the relatively large dispersion strength in the first chicane ISR may affect the performance of the echo seeding. The mechanism responsible for suppression of EEHG is diffusion in energy due to quantum fluctuations in the process of radiation. If the rms energy spread caused by this diffusion exceeds the spacing of two adjacent energy bands (see Fig. 3), the bands overlap and smear out the fine structures of the longitudinal phase space thus degrading the EEHG modulation.

One can easily estimate the energy diffusion by calculating the energy spread $\Delta\sigma_E$ due to passage of a charged particle through a bend of length L and bending radius ρ [11]:

$$\Delta\sigma_E^2\big|_{ISR} = \frac{55e^2\hbar c}{48\sqrt{3}}\frac{L}{\rho^3}\gamma^7\,, \qquad (11)$$

where γ is the relativistic factor and $\hbar$ is the reduced Planck constant. A quick estimate shows that for the beam energy close to 1 GeV, the bending radius of a few meters and the length of order of a meter, the energy spread due to ISR can be of the order of few kiloelectronvolts, or even as small as a fraction of keV, and is smaller than the energy spread for the cases considered in the previous section. However, a steep dependence of $\Delta\sigma_E$ on the beam energy would limit application of the echo seeding for beam energies of many gigaelectronvolts, unless a very weak magnetic field is used in the chicanes.

If the density modulation of the beam occurs inside the magnets of the chicane, it would cause the coherent synchrotron radiation and a concomitant energy modulation inside the dispersive section, which may result both in the emittance growth of the beam and the distortion of the phase space structures required for the echo modulation. Fortunately, there is a strong suppression effect due to a smearing of such modulation caused by nonzero values of the parameters R_{51} and R_{52} inside the chicanes. Typically, the dominant smearing is due to R_{51}, and the suppression factor for a Gaussian transverse beam profile is [12, 13]

$$e^{-k_{\rm mod}^2 R_{51}^2 \sigma_x^2/2}\,, \qquad (12)$$

where $k_{\rm mod}$ is the wave number of the modulation and σ_x is the transverse rms size of the bunch in the magnet. For representative numbers $\sigma_x \sim 40$ μm, $R_{51} \approx 0.01$, one finds that modulation with the wavelengths less then ~ 1 μm will be extinguished and hence the CSR will be suppressed.

One has to keep in mind, however, that for non-Gaussian distribution functions the suppression may not be so effective as presented by (12). It is also important to understand that the mechanism behind the suppression is reversible, and an unwanted beam modulation may recover at a downstream location in the accelerator lattice [14]. Overall, the issue of CSR effects in EEHG might require further theoretical and experimental studies.

One can use Eq. (12) to establish an important tolerance on the quality of the magnetic field of the chicanes. An ideal chicane has $R_{51} = 0$ at the exit. According to (12) a leaking nonzero value of R_{51} from the chicanes can smear

out the microbunching generated in the system. This leakage should be carefully controlled and minimized at the level when it does not deteriorate the EEGH.

There are also other requirements on the system that should be satisfied in order not to destroy a small-scale echo microbunching. They are discussed in more detail in Refs. [9, 15, 16].

PERFORMANCES OF THE EEHG FEL

To illustrate a possible performance of the EEHG FEL [9] we again use parameters of the Fermi@Elettra FEL project for the case of 10 nm wavelength.

The energy modulation and dispersion strengths were chosen to be the same as described above to maximize the bunching factor for the 24th harmonic. The first modulator was chosen to be 135 cm long with the undulator period length of 15 cm. The input laser had a waist of 310 microns and the peak power of 64 MW. The corresponding energy modulation amplitude was $A_1 = 3$. The second modulator was 45 cm long and had just 3 undulator periods. The laser parameters were the same and the corresponding normalized energy modulation amplitude was $A_2 = 1$.

The simulation was performed with the upgraded code Genesis [17, 18]. The radiator undulator had a period of 5 cm and was divided into 6 sections of 2.5 m separated by 0.5 m drift for focusing and beam diagnostics.

During the simulation, the dispersion strength and power of the seed laser were finely tuned to maximize the bunching factor for the 24th harmonic at the entrance to the radiator. The evolution of bunching factor and radiation power are shown in Fig. 5. The significant enhancement of the performance using the EEHG scheme is clearly seen in Fig. 5b where the peak power of the 24th harmonic radiation exceeds 1.6 GW and it saturates after 5 undulator sections (the total magnet length is 12.5 m). The large bunching factor at the entrance to the radiator offered by the EEHG scheme is responsible for the initial steep quadratic growth of the power. The high peak power and short saturation length should be attributed to the initial large bunching factor and the small energy modulation in the modulators. Indeed, the local energy spread at the entrance to the radiator is only about 2.45 times larger than the initial local energy spread.

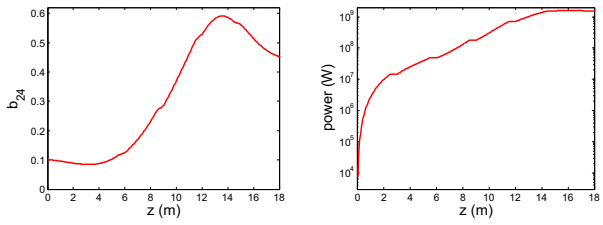

Figure 5: (a) Bunching factor vs radiator distance for the 10 nm radiation; (b) Peak power vs radiator distance for the 10 nm radiation.

With the same beam and laser parameters, the performance of an EEHG FEL was also simulated at the 48th harmonic, with the radiation wavelength of 5 nm. The results of that simulation can be found in Ref. [9].

In Ref. [19] a feasibility of coherent soft x-ray generation in the water window with the EEHG scheme was studied for the beam parameters based on the high repetition rate soft x-ray FEL under design at LBNL [20]. The parameters of the model are summarized in Table 2. The study assumed the seed laser wavelength of 190 nm with the EEHG FEL operating at the 50th harmonic of the laser. In order to limit the dispersion strength of the chicanes to a moderate value to mitigate the incoherent synchrotron radiation effect while not degrading the FEL performance, the dimensionless modulation amplitudes were chosen: $A_1 = 3$ and $A_2 = 6$.

Table 2: Main beam parameters

Electron beam energy	2.411 GeV
Peak current	1 kA
Normalized emittance	0.7 mm mrad
Slice energy spread	95 keV
Modulator period length	20 cm
Seed laser peak power	110 MW
Radiator period length	4 cm

Using the particle distribution obtained in a start-to-end simulation, it was demonstrated that the single-stage EEHG FEL can generate high power soft x-ray radiation in the water window with narrow bandwidth close to the Fourier transform limit directly from a UV seed laser. The output power profiles and spectrums corresponding to 3 different seed positions along the bunch obtained through time-dependent simulation using GENESIS code are shown in Fig. 6. The output pulse length is about 12 fs (rms) and the relative spectral bandwidth is 2.7×10^{-4}, about 1.3 times larger than the Fourier transform limit.

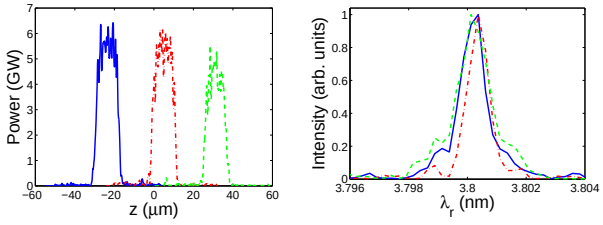

Figure 6: (a) Power profiles corresponding to different seed positions along the bunch; (b) Corresponding spectrum profiles.

The two examples explored soft x-ray FELs for the parameters of the machines that are constructed or being planned at this time. A preliminary feasibility study of a future hard x-ray FEL based on a two-stage EEHG concept is carried out in Ref. [21].

GENERATION OF ATTOSECOND PULSES WITH ECHO

As a further development of the EEHG scheme, in reference [22], it was shown that ultrashort pulses of x-ray radiation can be generated by adding a few more elements to the original scheme of the echo modulation. The schematic of the proposed set up is shown in Fig. 7. In this scheme,

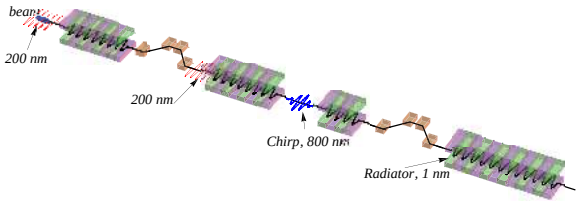

Figure 7: Schematic of the proposed scheme for generation of isolated attosecond x-ray pulse.

a short undulator is added before the second chicane, with a few-cycle laser beam tuned to the wavelength of the new undulator.

The beam interacts in the third undulator with a few-cycle intense laser whose wavelength is chosen to be much longer than that of the laser in the first two undulators, so that part of the electrons around the zero crossing of the few-cycle laser gets almost linear energy chirp. For the parameters considered in [22], the wavelength of the main seed laser was assumed 200 nm, and the wavelength of the additional laser was 800 nm. The energy of the 800 nm laser was 1 mJ and the pulse length 5 fs. With this additional energy chirp, the beam is longitudinally compressed after passing through the second dispersion section and the harmonic number is increased by the compression factor. In addition to assisting in extension of the harmonic number to a few hundred, the few-cycle laser also offers a possibility to select an isolated attosecond pulse. The result

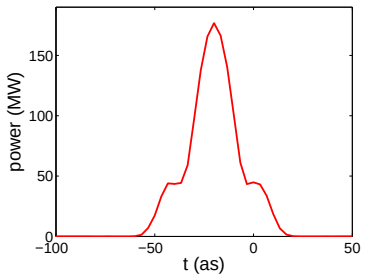

Figure 8: Power of the generated 1 nm x-ray pulse. The pulse length is 20 as (FWHM).

of simulations [22, 23] for the power output at 1 nm wavelength is shown in Fig 8. The peak power is about 180 MW, and the pulse length is about 20 as (FWHM).

In a recent paper [24] an echo-based scheme to generate two attosecond x-ray pulses with different carrier frequencies and variable delay has been proposed for x-ray stimulated Raman spectroscopy.

GENERATION OF TERAHERTZ RADIATION

A modification of the echo scheme [25] can be used to generate enhanced narrow-band terahertz (THz) radiation through down-conversion of the frequency of optical lasers using laser-modulated electron beams. The scheme is similar to the one shown in Fig. 1 except that now one has only one dispersion section and the aim is to down-convert the frequency of the lasers to generate THz modulation in the relativistic beam.

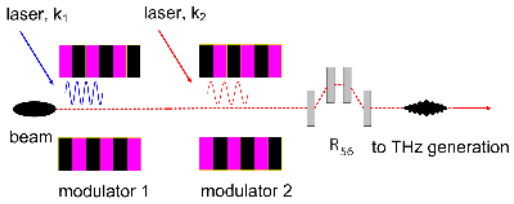

Figure 9: Scheme for generation of density modulation in electron beam.

In this scheme the frequencies of the lasers ω_1 and ω_2 are chosen in such a way that for some integers n and m the combination frequency $\omega = n\omega_1 + m\omega_2$ correspond to the terahertz frequency range. This means that one can generate density modulation at THz frequency in the beam using optical lasers. This density-modulated beam can be used to generate powerful narrow-band THz radiation. Since the THz radiation is in tight synchronization with the lasers, it should provide a high temporal resolution for the optical-pump THz-probe experiments. The central frequency of the THz radiation can be easily tuned by varying the wavelength of the two lasers and the energy chirp of the electron beam. The proposed scheme is in principle able to generate intense narrow-band THz radiation covering the whole THz range and offers a promising way towards the tunable intense narrow-band THz sources. In addition to generation of THz radiation, the density modulated beam can also be used to enhance the performance of the plasma wake field accelerators [26, 27].

In an example considered in Ref. [25] the wavelengths of the lasers are assumed to be 800 nm in the first modulator and 1560 nm in the second modulator. For the harmonic numbers $n = 1$ and $m = -2$, the generated modulation has a frequency of 10 THz. The electron beam has an energy of 60 MeV with a Gaussian distribution with rms bunch length of 0.5 ps, peak current of 200 A, and slice energy spread of 10 keV. Assuming $A_1 = 3$, it was found that the parameters that maximize the bunching factor were $A_2 = 5.74$ and $B = 19.95$ (corresponding to $R_{56} = 14.67$ mm). The

resulting beam current distribution and bunching factor for the laser-modulated beam are shown in Fig. 10. One can see that the laser-modulated beam was able to extend the THz radiation to 10 THz.

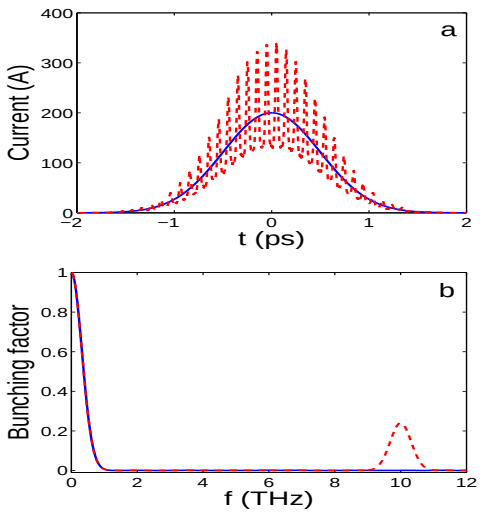

Figure 10: (a) Initial current distribution (solid blue line) and that after the dispersion section (dashed red line); (b) Corresponding bunching factor for the initial current distribution (solid blue line) and that after the dispersion section (dashed red line).

Terahertz radiation can be generated using transition radiation when the electron beam passes through a metallic foil. It was calculated in Ref. [25] that the peak radiation intensity is about 3 μJ/THz and peak power at 10 THz is about 0.33 MW. This powerful narrow-band THz radiation should have wide applications in THz imaging, nonlinear spectroscopy, etc. Since the THz radiation is in tight synchronization with the lasers, it should provide a high temporal resolution for the optical-pump THz-probe experiments.

PROOF-OF-PRINCIPLE EXPERIMENT AT SLAC

A proof-of-principe experiment to demonstrate EEHG is currently being planned at SLAC National Accelerator Laboratory. The existing NLCTA facility which houses an S-band photocathode electron gun and an X-band accelerator will be used for the experiment. The parameters of the experiment are summarized in Table 3. In the experiment, the beam will first be energy modulated in the first modulator using a Ti:Sapphire laser with the wavelength 785 nm and then sent through a chicane with a strong dispersion. A second laser from the optical parametric amplifier (1570 nm) will be used to further modulate the beam energy in the second modulator. As a result of the echo induced modulation, 7th harmonic of the second laser (224 nm) will be generated in the beam. The spectrum of the coherent OTR signal at this harmonic will be measured with a high-resolution optical-UV spectrometer as a function of the dispersion strength of the chicanes and the results will be used to benchmark the theory and simulations.

Table 3: Main beam and laser parameters

Electron beam energy	120 MeV
Normalized emittance	$< 8\,\mu$m
Slice energy spread	< 10 keV
First laser wavelength	785 nm
Second laser wavelength	1570 nm

CONCLUSIONS

The proposed approach of echo-enhanced harmonic generation provides a new promising way to introduce a controlled density modulation in an electron beam at a high harmonic of the laser frequency. It opens new possibilities in generation of coherent soft x-rays from free electron lasers, with an option that includes extremely short, attosend-duration pulses. It can also be used for generation of intense narrow-band THz radiation covering the whole THz range.

ACKNOWLEDGEMENTS

The author would like to thank his collaborator Dao Xiang, who made crucial contributions to many subjects covered in this report, and Zhirong Huang for many useful discussions.

This work was supported by the U.S. Department of Energy contract DE–AC02–76SF00515.

REFERENCES

[1] C. Pellegrini, in *Proc. European Particle Accelerator Conference, Edinburgh, 2006* (2006), pp. 3636–3639.

[2] A. Kondratenko and E. Saldin, Particle Accelerators **10**, 207 (1980).

[3] R. Bonifacio, C. Pellegrini, and L. M. Narducci, Optics Communications **50**, 373 (1984).

[4] R. Bonifacio, L. D. S. Souza, P. Pierini, and E. T. Scharlemann, Nucl. Instrum. Meth. **A296**, 787 (1991).

[5] L. Yu, Phys. Rev. A **44**, 5178 (1991).

[6] J. Wu and L. H. Yu, Nucl. Instrum. Meth. **A475**, 104 (2001).

[7] E. Allaria and G. D. Ninno, Phys. Rev. Lett. **99**, 014801 (2007).

[8] G. Stupakov, Phys. Rev. Lett. **102**, 074801 (2009).

[9] D. Xiang and G. Stupakov, Phys. Rev. ST Accel. Beams **12**, 030702 (2009).

[10] C. J. Bocchetta *et al.*, *Conceptual Design Report for the FERMI@Elettra*, Report ST/F-TN-07/12, ELETTRA (2007).

[11] A. W. Chao and M. Tigner, *Handbook of Accelerator Physics and Engineering* (World Scientific, Singapore, 2006), 3rd ed.

[12] S. Heifets, G. Stupakov, and S. Krinsky, Phys. Rev. ST Accel. Beams **5**, 064401 (2002).

[13] Z. Huang and K.-J. Kim, Phys. Rev. ST Accel. Beams **5**, 074401 (2002).

[14] Z. Huang *et al.*, in *Proceedings of the 2009 FEL Conference, paper WEOA01*, Liverpool, UK (2009).

[15] Z. Huang, D. Ratner, G. Stupakov, and D. Xiang, *Effects of energy chirp on echo-enabled harmonic generation free-electron lasers*, Preprint SLAC-PUB-13547, SLAC (2009).

[16] D. Xiang and G. Stupakov, *Tolerance Study for the Echo-Enabled Harmonic Generation Free Electron Laser*, Preprint SLAC-PUB-13644, SLAC (2009).

[17] S. Reiche, Nuclear Instruments and Methods in Physics Research **A429**, 243 (1999).

[18] S. Reiche, P. Musumeci, and K. Goldammer, in *Proceedings of the 2007 Particle Accelerator Conference* (IEEE, 2007).

[19] D. Xiang and G. Stupakov, *Coherent soft x-ray generation in the water window with the EEHG scheme*, Preprint SLAC-PUB-13645, SLAC (2009).

[20] J. Corlett *et al.*, Synchrotron Radiation News **22** (2009).

[21] D. Xiang, Z. Huang, and G. Stupakov, in *Proceedings of the 2009 FEL Conference*, Liverpool, UK (2009).

[22] D. Xiang, Z. Huang, and G. Stupakov, Phys. Rev. ST Accel. Beams **12**, 060701 (2009).

[23] D. Xiang, Z. Huang, D. Ratner, and G. Stupakov, in *Proceedings of the 2009 FEL Conference*, Liverpool, UK (2009).

[24] A. Zholents and G. Penn, *Obtaining two attosecond pulses for x-ray stimulated Raman spectroscopy*, CBP Tech Note 402, LBNL (2009).

[25] D. Xiang and G. Stupakov, Phys. Rev. ST Accel. Beams **12**, 080701 (2009).

[26] I. Blumenfeld *et al.*, Nature **445**, 741 (2007).

[27] P. Muggli, V. Yakimenko, M. Babzien, E. Kallos, and K. P. Kusche, Phys. Rev. Lett. **101**, 054801 (2008).